Proceedings of the 1999 IEEE
International Conference on Robotics & Automation
Detroit, Michigan • May 1999

Two-Dimensional Fine Particle Positioning Using a Piezoresistive Cantilever as a Micro/Nano-Manipulator

Metin Sitti and Hideki Hashimoto
Institute of Industrial Science, University of Tokyo
Roppongi, 7-22-1, Minato-ku, Tokyo, 106-8558, Japan

Abstract

In this paper, a fine particle positioning system using a pizoresistive cantilever, which is normally utilized in Atomic Force Microscopy, as the manipulator has been proposed. Modeling and control of the interaction forces among the manipulator, particle and surface have been realized for moving particles with sizes less than 3 μm on a Si substrate in 2-D. Optical Microscope (OM) is utilized as the vision sensor, and the cantilever behaves also as a force sensor which enables contact detection and surface alignment sensing. A 2-D OM real-time image feedback constitutes the main user interface, where the operator uses mouse cursor and keyboard for defining the tasks for the cantilever motion controller. Particle manipulation experiments are realized for 2.02 μm goal-coated latex particles, and it is shown that the system can be utilized in 2-D micro particle assembling.

1 Introduction

By the recent advances on micro-mechatronics technology, micro sensors and actuators, high precision positioners, micro robots inside the nuclear plant pipes, etc. have become possible. Especially, imaging devices such as Scanning Probe Microscopes (SPM) and Near-Field Optical Microscopes can provide imaging down to submicron and atomic scale at 2-D or 3-D. However, for constructing more complex micro/nano machines or devices by assembling micro/nano parts, necessary fabrication and manipulation technologies are still very immature at the scales less than 10 μm. Because, at these scales, micro/nano sticking forces become dominant to the inertial force, and a new robotics approach is indispensable. At this point, many researchers are trying to find new strategies for micro/nano assembly.

For the assembly of fine particles, different tools or control approaches have been proposed. For the particles sizes at the micro scale, Miyazaki et al. [1] proposed a two probe-based directly teleoperated assembly of spherical latex particles with the diameter of approximately 2 μm in 3-D, and tried to construct a 3-D pyramid where they had problems of assembling the last top particle due to adhesive forces. Tanikawa et al. [2] developed a directly teleoperated two-finger micro hand like a chopstick for moving glass spheres in 3-D with the size of 2 μm. Pappas et al. [3] proposed a robotics system where a micro/nano-tool is driven automatically for realizing simple tasks using visual servoing. They achieved positioning of 50 μm diameter diamond particles using a glass pipette with air pressure controlled picking and placing. For the nano scale particle manipulation, SPM probes such as Atomic Force Microscope (AFM) and Scanning Tunneling Microscope (STM) are utilized [4], [5], [6].

In this paper, a task-based semi-autonomous 2-D fine particle assembly system which utilizes piezoresistive AFM cantilever with its tip as the micro/nano manipulator and force sensor is proposed. As different from other works, the proposed system has the potential of also manipulating the nano objects by replacing the optical microscope imaging with the AFM non-contact imaging [7], the manipulator-particle contact is detected automatically using the real-time force feedback where the deformation of the tip or particle is prevented, even using one optical microscope, the depth (distance between the substrate/particle and cantilever) information is obtained through the cantilever substrate contact feedback, and manipulator-particle interaction forces during the manipulation are analyzed.

2 Problem Definition and Approach

Spherical polyvinyl gold-coated latex particles with sizes around 2.02μm (JEOL Datum Ltd.) are semi-fixed/absorbed to a Si substrate such that they are to be positioned by changing their xy positions [8], [9], [10]. The particles are also called as *absorbates*. The operations are to be realized in open air conditions with high relative humidity ($20 - 60\%$). Thus, the sticking forces such as capillary and van der Waals are strong. Here, it is assumed that the electrostatic

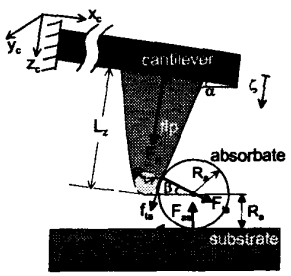

Figure 1: Positioning of the micro particles using the AFM tip as the manipulator.

forces are negligible with respect to other forces.

The cantilever tip which has a radius $R_t \approx 30nm$ is being utilized in contact pushing and pulling of the particles. Assuming the tip is pushing from a contact point passing through the absorbate center, the 3-D system can be simplified to 2-D as shown in Figure 1. The extension of the formulation to the 3-D case without assumption is direct. In the figure, F_{ta} and f_{ta} correspond to the tip-absorbate attractive/repulsive interaction force and friction force respectively. F_{as} and f_{as} are the interaction and friction forces for the absorbate and the substrate. The angle between the contact point of the tip and particle center is represented as β. The tip is aligned with an angle α. The tip is placed above the substrate with the parking height equals to the radius of the particle R_a. Thus, it is assumed not to touch to and interact with the substrate. By this way, the tip is not deformed, and vertical sticking force between the tip and particle is reduced.

Here, not the tip base but the substrate is moved with a constant speed V, and the manipulation strategy is as follows: *use the fixed cantilever as a stopper while moving the substrate under the particle with a uniform speed.* For fixing the particles, following conditions should be held:

- *at non-contact:* when the tip approaches or retracts from the particle, the particle should not stick to the tip and not move such that

$$\begin{aligned} F_{ta}sin\beta &\leq F_{as}, \\ f_{as} &\geq F_{ta}cos\beta, \end{aligned} \tag{1}$$

- *at contact:* when the tip contacts with the particle the resulting pushing or pulling force should be enough to fix the particle without breaking the tip, and flipping away the particle such that

$$\begin{aligned} &f_{ta}cos\beta + F_{ta}sin\beta \geq F_{as}, \\ &f_{as} \leq F_{ta}cos\beta - f_{ta}sin\beta. \end{aligned} \tag{2}$$

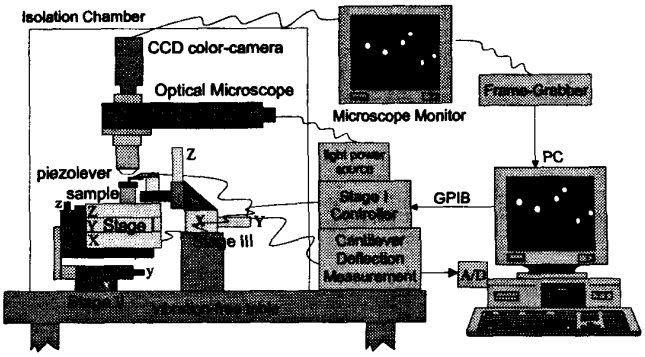

Figure 2: Overall system setup for the micro particle assembly.

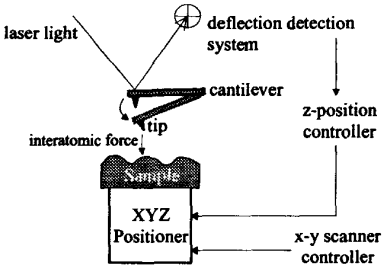

Figure 3: The basic structure of a conventional AFM.

The aim is to design the control parameters such as the contact point and angle, cantilever properties such as stiffness and tip radius and shape, particle-substrate friction, adhesion forces, humidity level and motion resolution and speed so that the above conditions can be held for a reliable manipulation.

3 System Setup

A task-based teleoperation control approach is selected where an operator determines the tasks to be realized, and a controller realizes these tasks automatically. The overall system is shown in Figure 2.

3.1 AFM as the Manipulator and Sensor

The basic structure of a conventional AFM system is shown in Figure 3. The very sharp cantilever tip atoms are interacted with the sample atoms by moving the sample/cantilever in the z-direction. The interatomic force $F_n(t)$ is attractive or repulsive, and the resulting typical deflection curve of the cantilever $\zeta(t)$ depending on the tip-sample distance $h(t)$ is shown in Figure 4. If the sample is moved slowly, i.e. the cantilever is assumed to be at equilibrium at each point:

$$F_n(t) = k_c\zeta(t), \tag{3}$$

where k_c is the previously known cantilever spring constant. Thus, the tip-sample force can be measured

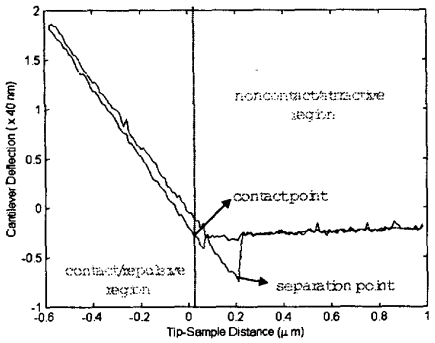

Figure 4: The typical cantilever deflection, i.e. interatomic force, and tip-sample distance relation for Si sample (experimental).

by measuring $\zeta(t)$. Instead of a laser interferometry-type deflection detection system, $\zeta(t)$ is measured by a Wheastone bridge-based deflection measurement electronics in our system since a piezoresistive cantilever (Park Scientific Instruments Co.) [11] is used. Thus, the output of the bridge is a voltage difference $V_{out}(t)$, and the nanometer value of the $\zeta(t)$ is computed from the below equation:

$$\zeta(t) = SG_2(G_1 V_{out}(t) + V_{off}), \qquad (4)$$

where $G_1 = G_2 = 100$ are the amplification gains, V_{off} is the offset voltage which is needed when there is an offset depending on the different resistance values of the cantilevers, $V_0 = 2.5V$ is the bridge voltage, and S is the constant scaling ratio which is calibrated for each cantilever previously.

Using the Eq. (3) and $F_n(t)$ vs. $h(t)$ relation curve, if a reference ζ^* is set at the contact linear region, then the z-stage is moved until detecting this point, and the (x, y) positions are scanned and at each point the same reference is tracked. Thus, the surface 3-D topology image can be held. This method is called *Contact Imaging Mode.*

Besides of being the 2-D contact push-pull manipulation tool, sensory functions of the AFM are as follows:

- $F_n(t)$ force feedback is held in real-time,
- the alignment error of the substrate can be compensated by getting a contact 3-D topology planar image of the substrate along single x and y lines where there is no particle,
- the contact between the tip and the particle can be detected by measuring $\zeta(t)$.
- the depth information can be obtained through the cantilever substrate contact feedback.

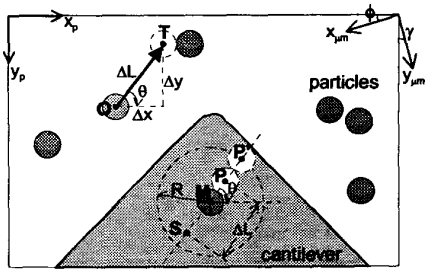

Figure 5: Automatic pushing or pulling operation, and image and positioner coordinates.

3.2 Vision Sensor: Optical Microscope

A reflecting light-type Optical Microscope (OM) (Olympus Co.) is used as the top-view vision sensor. It has approximately $\times 5000$ monitor magnification with $\times 80$ lens magnification, and $25mm$ working distance. A color camera (Sony Co.) on the OM is connected to a Matrox Co. Meteor frame-grabber which enables real-time color image viewing of the micro world on the PC screen with the range of 640×480 pixels in the image frame, (x_p, y_p), and approximately $57 \times 45\mu m^2$ in the world coordinates, $(x_{\mu m}, y_{\mu m})$. Hereafter, the world coordinates mean the coordinate frame for the AFM positioner x-y motion space. The image and world coordinate frames are given in Figure 5. In the case of linear mapping between both spaces, $x_{\mu m} = p_x x_p$ and $y_{\mu m} = p_y y_p$ where $p_x = p_y \approx 95nm/pixel$ are constant x and y scaling constants. However, during the experiments, it is observed that there is also some rotation in the coordinates due to the orientations of the camera, stage and sample surface. Therefore, a calibration process is needed before the experiments in order to map (x_p, y_p) to $(x_{\mu m}, y_{\mu m})$ which is explained later.

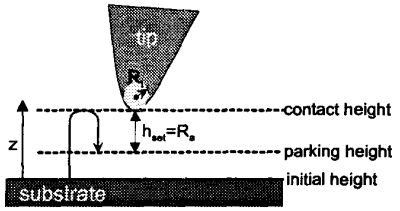

Figure 6: Parking height setting for the tip.

3.3 User Interface

The user interface constitutes of the real-time display of the top-view images from the camera mounted on the OM. The operator uses the mouse cursor and keyboard for defining the tasks for the AFM position controller. At present there are three main tasks:

- *Task 1 (T1)*: position the tip above the substrate,

- *Task 2 (T2)*: point-to-point relative motion,
- *Task 3 (T3)*: automatic pushing or pulling.

At the task T1, the tip is set to the height of R_a above from the substrate automatically. For this, the substrate is moved along the z-direction until touching to the tip, i.e. tip deflection is measured as ζ_{set}, then retracted back to the z-position given as $z = z_{final} - h_{set}$ where $h_{set} = R_a$ as shown in Figure 6.

In the task T2, using the mouse cursor, the operator clicks a point and its target point to be moved. Then the positon controller automatically moves with the amount of relative distance between the two points. This operation is needed for searching and initially positioning the particles on the screen.

The task T3 is used for semi-autonomous particle pushing or pulling. Freezing the continuous image, the operator selects the particle to be moved by clicking on the particle. Using image processing, the particle center **O** is automatically located. Next, the target position **T** is clicked by the operator. Then the pushing or pulling operation is realized automatically as shown in Figure 5 by the following strategy:

- *Step 1:* the tip radius R_t and center position **M**, particle center position **O** and radius R_a, and the target position **T** are computed or known,
- *Step 2:* compute the relative distance and orientation between **O** and **T** such that

$$\begin{aligned} \Delta x = x_T - x_O,\ \Delta y = y_T - y_O, \\ \theta = tan^{-1}(|\Delta y|/|\Delta x|), \\ s_x = \Delta x/|\Delta x|,\ s_y = \Delta y/|\Delta y|, \end{aligned} \quad (5)$$

- *Step 3:* find the point **P'** which is the initial set point before tip-particle contact such that

$$\begin{aligned} x_{P'} &= x_M + s_x R cos\theta, \\ y_{P'} &= y_M + s_y R sin\theta, \\ R &= R_t + 3R_a, \end{aligned} \quad (6)$$

- *Step 4:* move the tip $3R_a$ upward from the substrate for avoiding any possible collision between the tip and particle,
- *Step 5:* move from the point **O** to **P'**,
- *Step 6:* move back the tip to its parking height using T1,
- *Step 7:* find the contact point **P** by moving from **P'** through **M** by measuring the cantilever deflection,
- *Step 8:* find the point **S** where

$$\begin{aligned} x_S &= x_P - s_x \Delta L cos\theta, \\ y_S &= y_P - s_y \Delta L sin\theta, \\ \Delta L &= (\Delta x^2 + \Delta y^2)^{1/2}, \end{aligned} \quad (7)$$

- *Step 9:* move from **P** to **S**,
- *Step 10:* move from **P** to **T**.

In above operations, since the tip cannot be seen from the top view (it is approximately 7 μm inside from the end of the cantilever), the tip center **M** is computed roughly by using the Si substrate as a mirror, and then precisely by several particle contact tests.

3.4 Position Control

For the manipulation of the particles and initial settings, three different XYZ stages are utilized as shown in Figure 2. Stage I, the fine positioning XYZ piezoelectric stage (Physick Instrumente Co.) with 10 nm resolution, integrated LVDT (Linear Variable Differential Transformer) sensors, 100 μm range in all axes, %0.1 linearity error, and closed-loop PI control is utilized during the automatic particle assembly control. The other two stages are used for initial alignment and particle search on the surface. The main motion of the stage is point to point motion. Depending on the desired speed V, stairwise point-to-point motion is utilized for controlled manipulation speed where for moving from (x_1, y_1) to (x_2, y_2) point:

$$\begin{aligned} x_i &= x_1 + s_x \Delta cos\theta i, \\ y_i &= y_1 + s_y \Delta sin\theta i \end{aligned} \quad (8)$$

where $i = 1, \ldots, N$, $N = \Delta L/\Delta$, Δ is the predetermined motion step resolution, s_x, s_y, θ and ΔL are computed as the equations (5) and (7) for the case of $\Delta x = x_2 - x_1$ and $\Delta y = y_2 - y_1$. Thus, at each i^{th} step, firstly x_i then y_i is moved.

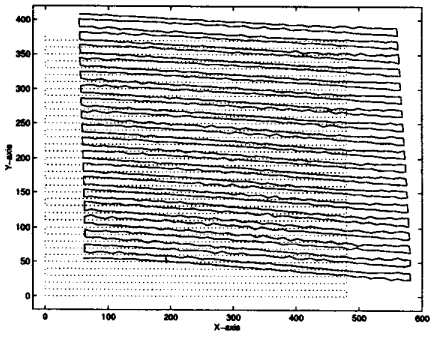

Figure 7: Controlled x-y scanning of the Stage I (dotted lines with 10 times magnification), and resulting detected particle center positions (solid lines).

3.5 Coordinate Frame Calibration

Image to world coordinates transformation constitutes of scaling and rotation transformations. Rotation transformation is due to the misalignment of the

substrate surface and OM image plane, and pan and tilt errors due to the rough manual positioner. For this purpose, a selected particle is tracked automatically during a controlled x-y motion. Particle detection image processing part is the same with the selection of the particle procedure. As an example, a scanning motion with 1 μm steps and 0.1% hystheresis error results in the particle center positions as shown in Figure 7.

From the calibration tests, the rotation angles ϕ and γ for the x and y axes, and scaling factor $p = p_x = p_y$ are computed. Then, the pixel to μm position trasformation is as follows:

$$\begin{aligned}
&\mathbf{x_{\mu m}} = \mathbf{A x_p},\\
&\mathbf{A} = \begin{bmatrix} -pcos\phi & psin\gamma & 640pcos\phi \\ psin\phi & pcos\gamma & -640psin\phi \\ 0 & 0 & 1 \end{bmatrix},\\
&\mathbf{x_{\mu m}} = [x_{\mu m} \quad y_{\mu m} \quad 1]^T,\\
&\mathbf{x_p} = [x_p \quad y_p \quad 1]^T. \qquad (9)
\end{aligned}$$

4 Analysis of Interaction Forces

For getting the conditions of the equations (1) and (2), non-contact and contact forces are analyzed. In this analysis, it is assumed that the contacting point of the cantilever tip behaves as a sphere of radius R_t during the force interaction while the whole tip shape is taken as a cone (that is the real case in our cantilever), electrostatic forces are negligible, and objects can be deformable. Furthermore, as the notation, '+' forces mean attractive, and '−' ones do the repulsive forces. Those conditions can be analyzed in two parts:

4.1 At Non-Contact

In this case, the tip is approaching to the particle. Then $f_{ta} = 0$, and F_{ta}, F_{as} and f_{as} can be modeled using the capillary and van der Waals forces, and JKR contact deformation model [12] as follows:

$$\begin{aligned}
&F_{as} = 4\pi\gamma R_a,\\
&F_{ta}(h(t)) = \frac{H\widetilde{R}}{6h^2} + \frac{2\pi\gamma\widetilde{R}cos\delta}{1+\frac{(h(t)-a_0)}{2r_1}},\\
&f_{as} = \mu F_L + cA_{as},\\
&A_{as}^3 = \frac{R_a}{K}\left(F_L + 6\pi R_a\gamma + \sqrt{12\pi R_a\gamma F_L + (6\pi R_a\gamma)^2}\right),\\
&F_L = F_{as} - F_{ta}sin\beta, \qquad (10)
\end{aligned}$$

where γ is the water surface energy, $h(t)$ is the tip-absorbate distance, r_1 is the meniscus curvature radius, H is the Hamacker constant (for the case of a liquid layer on the sample, $H = \{(H_{tip} - H_{liquid})(H_{sample} - H_{liquid})\}^{1/2}$ [12]), $\widetilde{R} = R_aR_t/(R_a + R_t)$, $a_0 = 30^{-1/6}\sigma$ is the contact point where σ is the interatomic distance, $K = 4/(3\pi)((1-\nu_t^2)/E_t + (1-\nu_p^2)/E_p)^{-1}$ is the equivalent Young modulus where E_t and E_p are the Young modulus and ν_t and ν_t are the Poisson's coefficients of the tip and particle respectively, δ is the liquid contact angle, and μ and c are the scaling constants for the load and adhesion part of the friction force respectively [13], [8] . In the case of micro scale particle size, $R_a/R_t >> 1$, and $\widetilde{R} \approx R_t$. Furthermore, F_{ta} becomes maximum at $h = a_0$ such that $F_{ta}(max) \approx 2\pi\gamma R_t$. Assuming the vertical forces are balanced, i.e. F_L is negligible, the conditions become as:

$$\begin{aligned}
&2R_a \geq R_t sin\beta,\\
&R_t cos\beta \leq c\widetilde{K}R_a^{2/3}, \qquad (11)
\end{aligned}$$

where $\widetilde{K} = (4\pi^2\gamma^2K/3)^{-1/3}$. The first equality is correct for any β where $R_a >> R_t$. The second one depends on c, K, β and R_t and R_a. For the case of $R_a = 30R_t = 1\mu m$, $\gamma = 0.072J/m^2$, $K = 10GPa$, approximate result is $cos\beta \leq 2c$. For this case, $c \geq cos\beta/2$ for not moving the particle on the substrate.

4.2 At Contact

At contact pushing, the forces are:

$$\begin{aligned}
F_{ta}(x(t)) &= 2\pi\gamma R_t - 4\pi K'\sqrt{R_t}(a_0 + x(t)/cos\beta)^{3/2},\\
F_{as}(x(t)) &= 4\pi\gamma R_a - 4\pi K\sqrt{R_a}(a_0 + x(t)sin\beta/cos\beta)^{3/2},\\
f_{ta}(t) &= \mu' F_{ta}(t) + c' A_{ta}(t),\\
f_{as}(t) &= \mu F_{as}(t) + cA_{as}(t), \qquad (12)
\end{aligned}$$

where $x(t)$ is the horizontal sample motion which depends on the motion speed V and resolution Δ, K' is the modulus for the tip-particle interaction, and $A_{ta}(t)$ and $A_{as}(t)$ are the contact areas. Putting these forces inside the conditions, the below equality is obtained:

$$\begin{aligned}
(\mu' sin\beta - cos\beta \quad -\mu\mu' cos\beta)F_{ta}(t) \leq -cA_{as}(t) +\\
c' A_{ta}(t)(\mu cos\beta - sin\beta). \qquad (13)
\end{aligned}$$

Here, using any deformation models such as Hertz, JKR, DMT or Maugis-Dugdale [7] models $A_{as}(t)$ and $A(_{ta}t)$ can be written in terms of adhesive forces and loads. For example, using the Hertz model, $A_{as}(t) = (R_aF_{as}(t)/K)^{1/3}$ and $A_{ta}(t) = (R_tF_{ta}(t)/K')^{1/3}$. Putting these contact areas to the Eq. (13), the relation is nonlinear and complex. However, assuming not smooth tip and particle surface geometry, the friction terms due to the contact area can be neglected with respect to the Amonton's load-based friction such that $c, c' \to 0$. Then, the following simplified condition is held:

$$tan\beta \leq \mu + \frac{1}{\mu'}, \qquad (14)$$

where $\beta \in [0, \pi/2]$. This condition implements that μ' should be small and relatively μ should be large.

During the contact pushing, the cantilever bending force is important for understanding the pushing force and cantilever dynamics. At the equilibrium points, the contact forces deflect the cantilever along the z_c axis as:

$$k_c\zeta(t) = f_{ta}(t)cos\psi + F_{ta}(t)sin\psi) + \lambda(-F_{ta}(t)cos\psi + f_{ta}(t)sin\psi), \quad (15)$$

where $\lambda = 2L_x/L_z$ is the structural contstant of the cantilever with the cantilever length L_x and tip height L_z respectively, and $\psi = \beta - \alpha$ is the tip half angle ($\psi = 16.5^o$ in our conic tip). Assuming $f_{ta}(t) = \mu' F_{ta}(t)$, the following equality held from the Eq. (15):

$$F_{ta}(t) = \frac{k_c}{\mu'(cos\psi + \lambda sin\psi) + sin\psi - \lambda cos\psi}\zeta. \quad (16)$$

Thus, $\zeta(t)$ curves are directly proportional to the $F_{ta}(t)$ curves. Furthermore, there is also a torsional force τ_c on the cantilever due to the contact force along the y_c axis where it can not be measured by the present hardware.

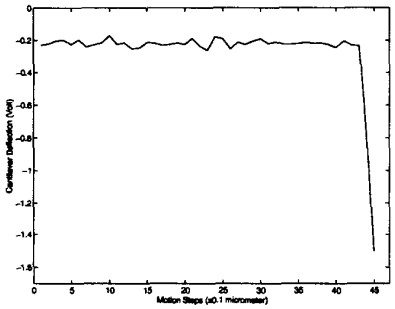

Figure 8: The cantilever deflection during automatic contact detection.

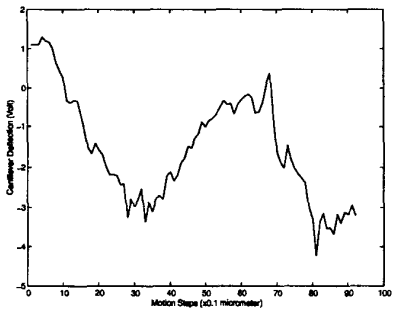

Figure 9: The cantilever deflection during pushing.

5 Experiments

As the first experiment, the contact point detection is tested. As the initial calibrations, the coordinate transformation parameters are computed as $p = 0.095$, $\phi = 9^o$, $\gamma = 1^o$, and the tip center is $(320, 304)pixel$. The cantilever parameters are $R_t = 30nm$, $S = 20nm/V$, $V_{off} = 3.62V$, and $k_c = 20N/m$, $L_x = 155\mu m$, and $L_z = 4\mu m$. The motion speed of the Stage I is around $V = 2\mu m/sec$ with $\Delta = 0.1\mu m$ steps. A particle is moved along a line that passes through the tip center, and $\zeta(Volt)$ is observed as in Figure 8. In the figure, $-0.2V$ is the no deflection line where around the 43^{th} step of motion the particle contacts and bends until to $-1.5V$ which is the ζ_{set} for automatic contact detection.

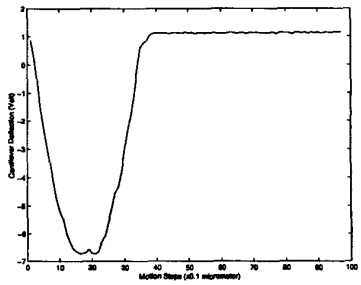

Figure 10: The tip and particle can lose the contact during pushing due to initial misalignment.

As the next experiment, the automatic pushing of two particles to form a line shape is realized as shown in Figure 11. The automatic pushing results can be seen in the figure where the particles are positioned to the user-defined target points. During pushing, one of the bending data of the cantilever, which also correspond to $F_{ta}(t)$, can be seen from Figure 9. From the figure, F_{ta} has some maximum points, F^*_{ta}, which correspond to the the separation points of the particle from the substrate. This phenomenon is caused by the shearing of the contact points [14] during the separation such that at these maxima:

$$f^*_{as} = -k_c S\zeta^* = \kappa A^*_{as} = F^*_{ta}(cos\beta - \mu' sin\beta), \quad (17)$$

where κ is the shear stregth of the contact points, and ζ^* is the measured minima of the curve in Figure 9. In the figure, after breaking the bonds, since the cantilever contacts with the particle and breaks its bonds again, there are many peaks in the deflection curve such that $f^*_{as} = 1.2\mu N$ and $f^*_{as} = 1.6\mu N$ respectively. Also, the maximum contact areas can be calculated using the Eq. (17) such that $A^*_{as} = 0.0083\mu m^2$ and $0.011\mu m^2$ with the contact radii $51.5nm$ and $59.5nm$ respectively where $\kappa = 144 \times 10^6 N/\mu^2$ in the case of water layer between the particle and substrate.

In some cases, if the contact point of the particle and tip is not well centered, i.e. does not pass through the particle center, the particles can be pushed only once, and then the tip can lose its contact with the particle as shown in Figure 10. For avoiding this problem,

Δ is decreased for reducing positioning errors. Moreover, pushing can break the cantilever tip sometimes due to very large F_{ta}. This possibility is minimized by checking the ζ during pushing such that if it exceeds $-10V$, which is also the saturation voltage of the amplifier, then the pushing is stopped, and the design of the particle and substrate should be changed according to the force analysis by changing the environment parameters such as adding lubricants between the particle and substrate, realizing the manipulation in a liquid environment, etc.

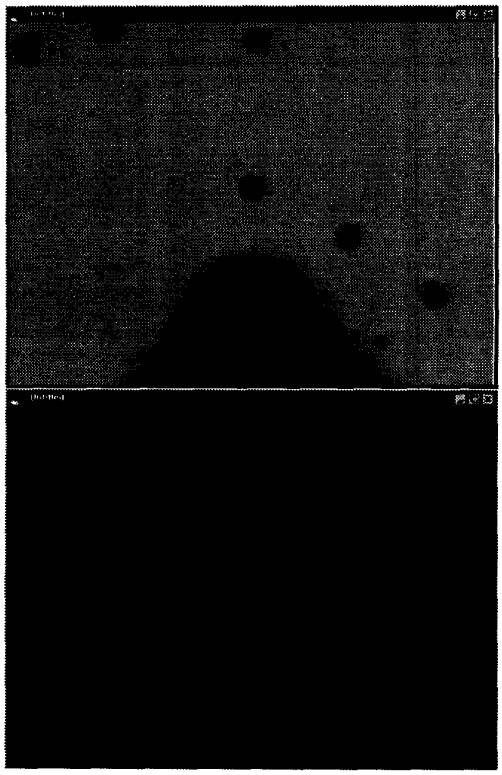

Figure 11: Pushing particle result: the initial positions (upper image), and the last configuration with the moved two particles (bottom).

6 Conclusion

In this paper, a micro particle manipulation system using a piezoresistive AFM cantilever as the manipulator and force sensor has been proposed. Modeling and control of the AFM cantilever tip and particle interaction has been realized for moving particles with sizes less than 3 μm on a Si substrate in 2-D. Particle manipulation experiments are realized, and it is shown that the system can be utilized in 2-D micro particle assembling. As the future work, the size of particles will be reduced down to 10s of nanometer, and the manipulation operations will be realized in a liquid environment where the capillary and electrostatic forces are reduced. Also, 3-D manipulation is aimed where special electromechanical MEMS or biochemical grippers can be used.

Acknowledgements

Authors would like to thank Park Scientific Instruments Co. for providing the piezoresistive cantilevers, and all other Hashimoto Lab. members for their various helps.

References

[1] H. Miyazaki and T. Sato, "Pick and place shape forming of three-dimensional micro structures from fine particles," in *Proc. of the IEEE Int. Conf. on Robotics and Automation*, pp. 2535–2540, 1996.

[2] T. Tanikawa, T. Arai, and T. Masuda, "Development of micro manipulation system with two-finger micro hand," in *Proc. of the IEEE/RSJ Int. Conf. on Intelligent Robots and Systems*, pp. 850–855, 1996.

[3] I. Pappas and A. Codourey, "Visual control of a microrobot operating under a microscope," in *Proc. of the IEEE/RSJ Int. Conf. on Intelligent Robots and Systems*, pp. 993–1000, 1996.

[4] D. Schafer, R. Reifenberger, A. Patil, and R. Andres, "Fabrication of two-dimensional arrays of nanometric-size clusters with the atomic force microscopy," *App. Physics Letters*, vol. 66, pp. 1012–1014, Feb. 1995.

[5] A. A. Requicha, C. Baur, and et al., "Nanorobotics assembly of two-dimensional structures," in *Proc. of the Workshop on Precision Manipulation at the IEEE Robotics and Autom. Conf.*, pp. 136–150, 1998.

[6] J. Stroscio and D. Eigler, "Atomic and molecular manipulation with the scanning tunneling microscope," *Science*, vol. 254, pp. 1319–1326, Nov. 1991.

[7] M. Sitti and H. Hashimoto, "Tele-nanorobotics using atomic force microscope," in *Proc. of the IEEE/RSJ Int. Conf. on Intelligent Robots and Systems*, pp. 1739–1746, Canada, Oct. 1998.

[8] M. Sitti and H. Hashimoto, "Macro to nano telemanipulation through nanoelectromechanical systems," in *Proc. of the IEEE Ind. Electronics Conf.*, pp. 98–103, Germany, Sept. 1998.

[9] M. Sitti, K. Hirahara, and H. Hashimoto, "2-d micro particle assembly using atomic force microscope," in *Proc. of the IEEE Int. Symp. on Micro Machine and Human Science*, pp. 143–148, Nagoya, Nov. 1998.

[10] M. Sitti and H. Hashimoto, "Two-dimensional fine particle positioning under optical microscope using a piezoresistive cantilever as a manipulator," *J. of Micromechatronics*, 1999 (submitted).

[11] F. J. Giessibl and B. M. Trafas, "Piezoresistive cantilevers utilized for scanning tunneling and scanning force microscope in ultrahigh vacuum," *Rev. Sci. Instrum.*, vol. 65, pp. 1923–1929, June 1994.

[12] J. Israelachvili, *Intermolecular and Surface Forces*. Academic Press, 1992.

[13] A. Berman and J. Israelachvili, "Control and minimization of friction via surface modification," *Micro/Nano Tribology and its Application, Kluwer Academics Pub.*, pp. 317–329, 1997.

[14] C. M. Mate, "Force microscopy studies of the molecular origin of friction and lubrication," *IBM J. Res. Develop.*, vol. 39, pp. 617–627, Nov. 1995.